Air Entrainment into Mechanical Smoke Vent on Ceiling

Daisaku NII, Kuratoshi NITTA and Kazunori HARADA
Department of Architecture and Environmental Design, Kyoto University
Yoshida-Honmachi, Sakyo, Kyoto 606-8051, Japan

Jun'ichi YAMAGUCHI
Technical Research Institute, Obayashi Corporation
4-640, Simokiyodo, Kiyose, Tokyo 204-8558, Japan

ABSTRACT

Air entrainment ratio to mechanical ceiling vent was investigated by model scale experiments for quiescent two-layers environment. For various combinations of venting velocity and smoke layer temperature, critical smoke layer thickness for onset of entrainment was identified by eye-observation. Air entrainment ratio was measured by the change of carbon dioxide concentration in smoke layer (before entrainment) and in exhaust duct (after entrainment). By summarizing the measured results, the followings were clarified. 1) The critical thickness for onset of entrainment depends on smoke layer temperature and largely on smoke layer thickness. When the smoke layer is thick, large venting velocity is needed to cause air entrainment. In this condition, flow into vent opening can be approximated by potential flow to point sink. As the smoke layer thickness is decreased, relatively small venting velocity can cause air entrainment. In this condition, flow pattern can be approximated by potential flow to line sink or to plane sink depending on aspect ratio. 2) Even at the critical condition determined by eye-observation, certain amount of air is entrained. 3) Beyond the critical condition, air entrainment ratio can be approximated by the fraction of actual smoke layer thickness to critical smoke layer thickness for onset of visible air entrainment.

KEYWORDS: mechanical smoke venting, air entrainment, critical smoke layer thickness, aspect ratio, Froude number

INTRODUCTION

Mechanical smoke venting system is often equipped in large buildings in order to facilitate egress, rescue and fire fighting. In practical design, large venting flow rate is normally required in the code and standards [1,2], which often results in excessive venting velocity. In the two-layer environment, excessive venting velocity causes air entrainment into vent opening, which reduces the net exhaust rate of smoke. It is desirable to optimize number, size and geometry of smoke vent opening in order to prevent air entrainment.

However, common engineering tools such as BRI2 [3] and CFAST [4] do not take into account of the influence of air entrainment from lower zone in their mass and energy

balance equations. Concerning the air entrainment to smoke vent, most extensive study would be a series of experiments carried out by Spratt *et al* [5]. They changed the aspect ratio of rectangular vent openings to measure critical flow rate for the onset of air entrainment. They concluded that critical flow rate could be expressed by a function of smoke layer temperature and thickness. However, their results are not sufficient in that their experiments cover only one specific combination of smoke layer temperature and thickness (208^{o}C, 13.5cm) and that the aspect ratio of vent opening is limited in less than or equal to *eight*. Moreover, no information is given on the air entrainment ratio. In the area of hydraulics, Davidian *et al* [6] found similar correlations for the critical velocity for pumping up water from lakes.

The purpose of this study is to develop experimental formulae for air entrainment ratio under various combinations of aspect ratio, smoke layer thickness and temperature with an arbitrary velocity. The formulae are simple enough to be used in zone models. The prediction formulae are composed of two parts: 1) critical smoke layer thickness for given smoke layer temperature, venting velocity and aspect ratio, 2) air entrainment ratio according to the function of actual smoke layer thickness over critical smoke layer thickness. For formulation, dimensional analysis was carried out to correlate the variables. Then the formulae were correlated with the results of model scale experiments whose aspect ratio covers *one* to infinite.

THEORY

Consider a quiescent two-layer environment of air and smoke as shown in Fig. 1. Uniform temperature is assumed in each layer (T_s [K] in smoke layer and T_a [K] in air layer). Smoke vent opening is equipped on ceiling to exhaust smoke at average velocity v [m/s] (volume flow rate per unit area of vent opening). Under a given venting velocity, the onset of air entrainment depends on smoke layer thickness as shown in Fig. 1. When smoke layer is thick enough, the air-smoke interface is lifted up toward vent opening, but not entrained into vent opening as shown in Fig. 1a). As smoke layer thickness decreases, the stability of upper smoke layer is broken at a certain smoke layer thickness, which results in air entrainment as shown in Fig. 1b).

In the followings of this section, critical smoke layer thickness for the onset of entrainment $d_{s,cr}$[m] would be correlated with density difference $\Delta\rho(\equiv\rho_a-\rho_s)$ at given velocity v[m/s]. Simple potential flow theory was applied to describe air entrainment ratio beyond the critical condition.

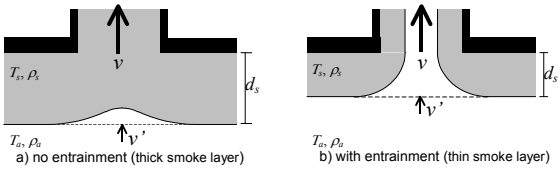

Figure 1 Typical Flow Patterns below Smoke Vent Opening

Critical Condition for the Onset of Entrainment

General Principle

Referring to Fig. 1, when the velocity of induced air to interface is v' [m/s], the specific momentum energy of induced air is $\rho_a v'^2/2$. If the momentum energy exceeds a certain limit, the induced air breaks the smoke layer to reach to vent opening. It is natural to consider that the limit is proportional with the potential energy increment. If we consider a unit volume of stationary air at the interface height, the work to bring this volume up through smoke layer against negative buoyancy force would be $\Delta\rho g d_s$. Thus it is expected that

$$\rho_a v'^2 / 2 \propto \Delta\rho g d_{s,cr} \tag{1}$$

would be applied to describe critical smoke layer thickness for the onset of entrainment.

To correlate the induced velocity v' with venting velocity v, mass balance is considered. As shown in Fig. 2, the control volume is considered to cover the opening with distance R [m]. Resulting shape consists of a combination of one rectangular parallel-piped, four quarter cylinders and four 1/8 of sphere.

Assuming that induced velocity over the control volume surface is uniform, and approximating that the influence of density change is small on mass conservation, induced velocity v' and venting velocity v are correlated by

$$vWH = v'\left\{WH + \pi R\left(W + H\right) + 2\pi R^2\right\}. \tag{2}$$

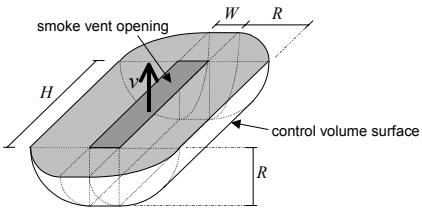

Figure 2 Control Volume for Flow below Smoke Vent (general case)

In the critical condition, air-smoke interface touches the bottom of control volume. Putting $R=d_{s,cr}$ and substituting Eq. 2 to Eq. 1, critical smoke layer thickness is related with venting velocity.

$$d_{s,cr}\left\{WH + \pi d_{s,cr}\left(W + H\right) + 2\pi {d_{s,cr}}^2\right\}^2 \propto \frac{v^2}{\Delta\rho g/\rho_a}\left(WH\right)^2 \tag{3}$$

Simplification According to the Range of Venting Velocity

General correlation Eq. 3 can be further simplified according to the range of venting velocity in consideration. As shown in Fig. 3, the critical thickness changes in accordance with venting velocity. When venting velocity is small, critical thickness is also small. In this case, control volume can be approximated by rectangular parallel-piped. As venting

velocity is increased, control volume can be approximated by a half-cylinder or by a hemisphere. For each pattern, flow into opening can be approximated by plane, line or point sink, respectively.

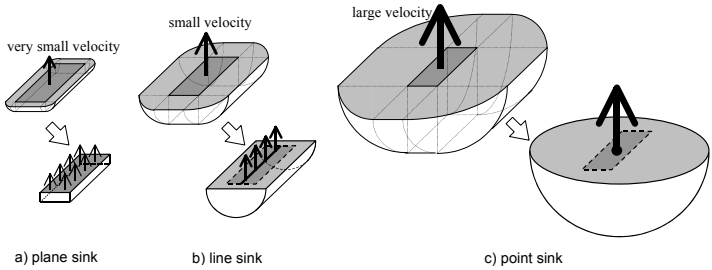

Figure 3 Variation of Control Volume by Venting Velocity

In the case of large venting velocity, the control volume is approximated by a hemisphere. Therefore the first and second terms in Eq. 3, $WH + \pi d_{s,cr}(W+H)$, are negligible in comparison with the last term $2\pi {d_{s,cr}}^2$. Rearranging terms and omitting a factor of 2π, we get

$$ {d_{s,cr}}^5 \propto \frac{v^2}{\Delta\rho g/\rho_a}(WH)^2 . \tag{4} $$

To get a non-dimensional expression using Froude number, short edge length of vent opening W was selected as a characteristic dimension. Thus, we get

$$ \frac{d_{s,cr}}{W} \propto \left(\frac{H}{W}\right)^{2/5}\left(\frac{v}{\sqrt{\Delta\rho g W/\rho_a}}\right)^{2/5} = (H/W)^{2/5}\, Fr^{2/5} . \tag{5} $$

Similar formulations were carried out. The final forms for the three flow patterns are

$$ \frac{d_{s,cr}}{W} \propto \begin{cases} Fr^2 & \left[\text{plane sink:dominated by } WH\right] \\ Fr^{2/3} & \left[\text{line sink:dominated by } \pi d_{s,cr}(W+H)\right] \\ (H/W)^{2/5}\, Fr^{2/5} & \left[\text{point sink:dominated by } 2\pi {d_{s,cr}}^2\right] \end{cases} . \tag{6} $$

The relationships in Eq. 6 are shown in Fig. 4. Flow pattern is determined by the range of Froude number and aspect ratio. As Froude number increases, flow pattern shifts from plane sink to line sink (A) and finally to point sink (B). In this sequence, the power on Froude number changes from 2, to 2/3 and then to 2/5 as shown by the solid line for a specific aspect ratio.

The branch to point sink varies in accordance with aspect ratio as shown by broken lines. In case that aspect ratio is equal to unity, flow pattern changes directly from plane sink to point sink. For other aspect ratios, the branch from line sink to point sink takes place at

$$Fr_{branch} \propto \left(H/W\right)^{3/2}, \tag{7}$$

which was derived by the formulae for line and point sink in Eq. 6.

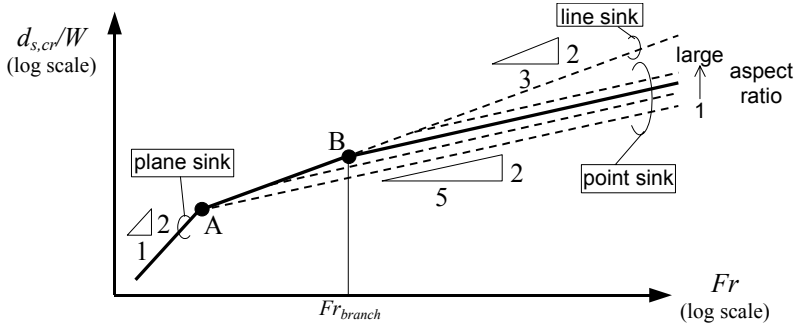

Figure 4 Transition of Flow Pattern

Air Entrainment Ratio

When the actual smoke layer is less thick than the critical thickness ($d_s<d_{s,cr}$) as shown in Fig. 5, air entrainment takes place. In such a condition, air entrainment ratio (fraction of entrained air volume over total venting volume) is to be predicted.

At first, flow pattern is determined by venting velocity and aspect ratio using Eq. 7. Then the critical thickness is calculated using Eq. 6. Assuming uniform induced velocity to control volume surface, air entrainment ratio for specified flow pattern is calculated by the ratio of surface area that contacts with air layer. Thus, we get

$$\phi = \begin{cases} 1 & \left[\text{plane sink}\right] \\ \left(2/\pi\right)\cos^{-1}\left(d_s/d_{s,cr}\right) & \left[\text{line sink}\right] \\ 1-\left(d_s/d_{s,cr}\right) & \left[\text{point sink}\right] \end{cases}. \tag{8}$$

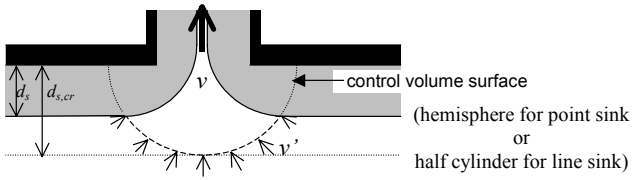

Figure 5 Area of Air Entrainment

EXPERIMENTS

To determine the coefficients of correlation in Eq. 6, and to verify the accuracy of prediction formula of air entrainment ratio in Eq. 8, model scale experiments were carried out.

Experimental Conditions

Experiments were planned in order to obtain critical conditions and air entrainment ratio for

several aspect ratios under various venting velocity and smoke layer temperature. Experimental conditions are shown in Tab. 1. Measurements were carried out also for the cases comparable with data by Spratt *et al*. Selected aspect ratios were 1, 2, 8, 13.3, 40 and infinite (slender opening with side walls along short edge). Venting velocity was changed in the range of 0.26-10.58 m/s. Corresponding temperature difference between smoke and air layers were in the range of 33.6-70.7 ^{o}C.

Table 1 Summery of Experimental Conditions

Aspect Ratio H/W	Vent Size W x H[cm]	Venting Velocity v[m/s]	Temperature Difference $\Delta T=T_s-T_a$ [K]	Number of Experiment
1	10 x 10, 20 x 20 25 x 25	0.26-6.03	41.3-59.5	24
2	10 x 20	0.52-2.92	42.0-54.6	9
8	5 x 40	0.68-2.80	42.8-59.9	8
13.3	3 x 40	1.23-4.36	36.5-70.7	8
40	1 x 40	5.00-9.78	37.3-69.9	9
Infinite (with side walls)	5 x 40, 1 x 40	1.19-10.58	33.6-59.6	28

Experimental Setup and Procedure

Schematic of experimental apparatus is shown in Fig. 6. The size of model room was 1,640mm wide x 900mm deep x 1,270mm high. Vent opening was equipped at the center of ceiling. Front wall was made of transparent PMMA board (2mm thick) for observation convenience. The other surfaces (ceiling, back wall and side walls) were made of plywood board insulated by 25mm thick ceramic-fiber board.

The smoke layer thickness and temperature were adjusted by changing the height of gas burner. Venting rate was adjusted by regulating the valve in the duct while being measured by orifice flow meter. When necessary, excess smoke was expelled through an opening by changing the depth of smoke curtain on the opposite side of gas burner. Smoke layer thickness and temperature were determined by vertical temperature profiles measured by a thermocouple tree.

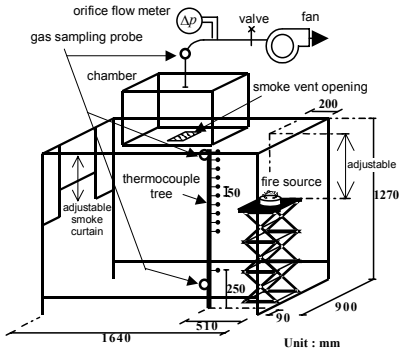

Figure 6 Experimental Apparatus

After the smoke layer thickness and temperature had stabilized, carbon dioxide

concentration was measured at three locations; smoke layer (Y_s), lower air layer (Y_a) and exhaust duct (Y_{duct}). Then the air entrainment ratio was calculated by

$$\phi = \left(Y_s - Y_{duct}\right) / \left(Y_s - Y_a\right). \quad (9)$$

Trial and error process was repeated to find the critical condition for the onset of air entrainment. For respective venting rate, artificial smoke (neutrally buoyant white chemical compounds) was released right below the air-smoke interface to see air entrainment.

RESULTS

Critical Smoke Layer Thickness for the Onset of Entrainment

Fig. 7 (right) shows visualized interface in one of the critical condition. The air-smoke interface is lifted beneath the vent opening. However, there is no visible entrainment of air into vent opening. When venting velocity was increased more, entrainment took place. The vertical temperature profile in this critical condition is shown in Fig. 7 (left). Using the vertical profile, air-smoke interface was determined by the crossing point of extrapolated line of steep change in smoke layer temperature with lower layer temperature. The smoke layer temperature was averaged among the measuring points above the interface.

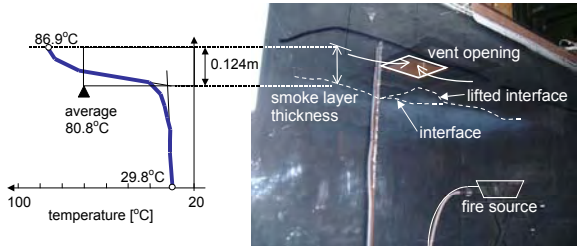

Figure 7 Lifting of interface at the critical condition for entrainment (right) and temperature distribution (left) (d_s=0.124 m, v=0.31 m/s, T_s=80.8 °C, T_a=29.8°C, opening size=25cm x 25cm)

Air Entrainment Ratio

As an example, measured results for the condition of previous section (Fig. 7) is described below. Measured carbon dioxide concentration values over the central plane were measured. The average yielded a value of 0.41%. Using the measured value in lower layer (Y_a=0.05%) and in the duct (Y_{duct}=0.35%), the air entrainment ratio was calculated by

$$\phi = \frac{Y_s - Y_{duct}}{Y_s - Y_a} = \frac{0.41 - 0.35}{0.41 - 0.05} = 0.17. \quad (10)$$

As the venting velocity is increased to v=0.40m/s, smoke layer thickness is a bit deceased to d_s=12.0cm. The air entrainment ratio was 0.22. On the other hand, the air entrainment ratio was decreased to 0.11 at smaller venting velocity (v=0.26m/s, d_s=12.7cm).

DISCUSSION

Critical Smoke-Layer Thickness

Measured critical smoke layer thickness were plotted versus Froude number in Fig. 8 together with published data by Spratt *et al*. Using these data, the coefficient of Eq.6 are determined in the following. With reference to Fig. 4, critical smoke layer thickness for line sink is invariantly larger than that for point sink. Therefore, the upper bound of the plot would correspond with line sink. Here, it was considered that encircled data in Fig. 8 corresponds with line sink. Other data would correspond with point sink. It is guessed that there is no data for plane sink neither in this study nor in Spratt's data because venting velocities were too large to produce plane sink.

Correlations for Line Sink

As was predicted by Eq. 6, critical thickness depends on 2/3 power of Froude number. As shown in Fig. 8, best correlation was obtained by

$$d_{s,cr}/W = 0.98Fr^{2/3}. \tag{11}$$

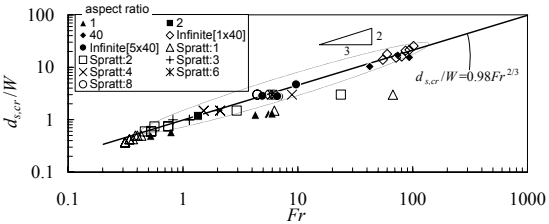

Figure 8 Correlations of Critical Smoke Layer Thickness and Froude Number in Case of Line Sink

Correlations for Point Sink

Following Eq. 6, data for point sink were plotted versus $(H/W)^{2/5}Fr^{2/5}$ as shown in Fig. 9. The measured results coincide with Spratt's data. All the data can be fit by one regression line with slope 2/5 following Eq. 6. The best correlation was obtained by

$$d_{s,cr}/W = 0.64\left(H/W\right)^{2/5} Fr^{2/5}. \tag{12}$$

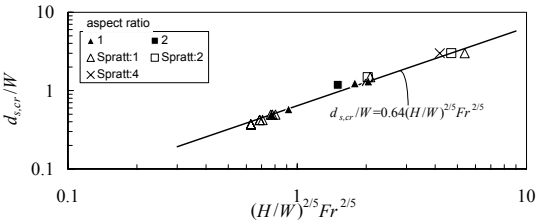

Figure 9 Correlations of Critical Smoke Layer Thickness and Froude Number in Case of Point Sink

Final Form for Critical Thickness

The final form of experimental formula is plotted in Fig. 10 with all the experimental data. The dotted lines in Fig. 10 correspond with Eq. 12 for point sink in case that aspect ratios are 1, 2 and 4. As the aspect ratio is increased, the branching Froude number is increased in accordance with

$$Fr_{branch} = 0.2\left(H/W\right)^{3/2}. \tag{13}$$

In the special case of (H/W)=1, Eq. 13 gives the smallest branching Froude number Fr=0.2. If the Froude number is less than 0.2, flow into vent opening would be plane sink. In this region, it is expected that the power on Froude number would be 2. In summary, the critical smoke layer thickness is well correlated by the following formula

$$\frac{d_{s,cr}}{W} = \begin{cases} 8.2Fr^2 & \left(0 \le Fr \le 0.2\right) & \left[\text{plane sink}\right] \\ 0.98Fr^{2/3} & \left(0.2 \le Fr \le 0.2\left(H/W\right)^{3/2}\right) & \left[\text{line sink}\right] \\ 0.64\left(H/W\right)^{2/5} Fr^{2/5} & \left(0.2\left(H/W\right)^{3/2} \le Fr\right) & \left[\text{point sink}\right] \end{cases}. \tag{14}$$

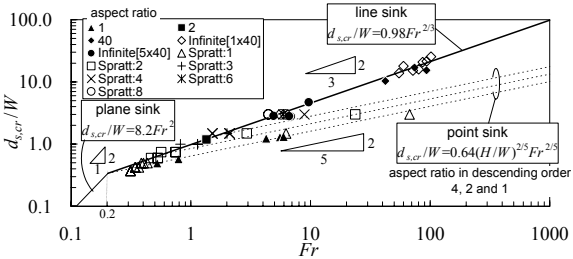

Figure 10 Correlations of Critical Smoke Layer Thickness and Froude Number for Three Flow Patterns

Air Entrainment Ratio

All the experiments were carried out for Froude numbers larger than 0.47. Judging from calculated Froude numbers, no data was classified into plane sink category. Thus, only the data for line sink and point sink were obtained. For each measurement condition (velocity and smoke-air temperature difference), Froude number was calculated. In the case that calculated Froude number is less than branching Froude number by Eq. 13, flow pattern was determined as line sink. In the case that Froude number exceeds branching Froude number, flow pattern was determined as point sink. In the following, correlations for line sink and point sink were obtained.

Air entrainment ratios are shown in Fig. 11 for line sink versus non-dimensional smoke layer thickness $d_s/d_{s,cr}$ as suggested by Eq. 14. Eq. 8 gives good agreement when non-dimensional smoke layer thickness $d_s/d_{s,cr}$ is small. As $d_s/d_{s,cr}$ is increased, agreement becomes worse. When $d_s/d_{s,cr}$ is over unity (beyond visible entrainment limit), Eq. 8 yields

no air entrainment ratio. However, measured results show that certain amount of air is entrained even beyond visible entrainment limit. In Fig. 12, data for point sink are plotted in the same way. Similar to the case of line sink, agreement is good only in small non-dimensional smoke layer thickness.

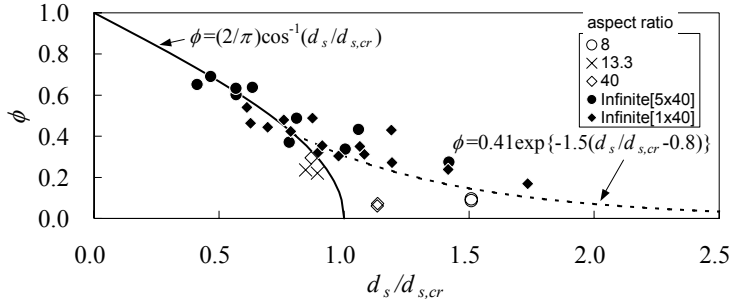

Figure 11 Comparisons between Prediction Formula and Experimental Data of Air Entrainment Ratio in Case of Line Sink

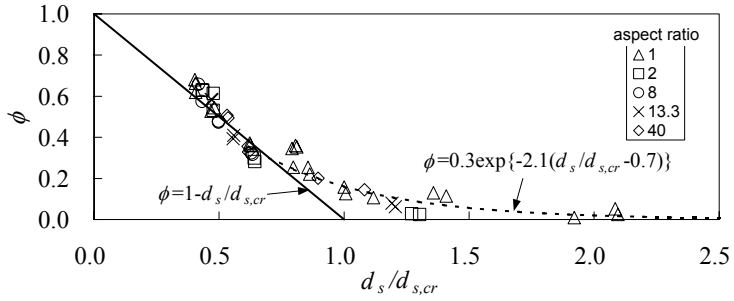

Figure 12 Comparisons between Prediction Formula and Experimental Data of Air Entrainment Ratio in Case of Point Sink

To cover over visible entrainment limit, simple curve fitting was carried out to yield:

$$\phi = \begin{cases} (2/\pi)\cos^{-1}\left(d_s/d_{s,cr}\right) & d_s/d_{s,cr} \le 0.8 \\ 0.41e^{-1.5\left(d_s/d_{s,cr}-0.8\right)} & d_s/d_{s,cr} > 0.8 \end{cases} \tag{15}$$

for line sink, and

$$\phi = \begin{cases} 1-d_s/d_{s,cr} & d_s/d_{s,cr} \le 0.7 \\ 0.3e^{-2.1\left(d_s/d_{s,cr}-0.7\right)} & d_s/d_{s,cr} > 0.7 \end{cases} \tag{16}$$

for point sink.

Consistency with Theoretical Assumptions

Assumption of Flow Patterns

To check the validity of the assumptions of flow patterns, the velocity distribution toward center of vent opening was measured. An example of results is shown in Fig. 13a). Vent size was 10cm x 10cm. The venting velocity was 2.45m/s. Smoke layer thickness was 13.2cm. Average smoke layer temperature was 71.1°C. The flow pattern for this case is determined as point sink.

There is a considerable difference in velocity. Maximum velocity arises at the point right below vent opening. The smallest velocity exists near ceiling part. The difference was approximately 30% against average velocity. As is demonstrated, the assumption of flow pattern is not very similar to point sink because of the obstruction by ceiling surface. However, the effect is included in the error bound in deriving experimental formula. Thus, it is not a very serious problem.

Visible Entrainment Limit

The distribution of CO_2 concentration for the same experiment as in previous section is shown in Fig. 13b). The experimental condition corresponds with visible entrainment limit. The measured entrainment ratio was 25%. As shown in this figure, low concentration part builds up like a mountain toward the center of vent opening. Even it could not be seen by eye, but certain amount of air entrainment is suspicious. In addition, turbulent mixing at the smoke-air interface might increase the entrainment rate.

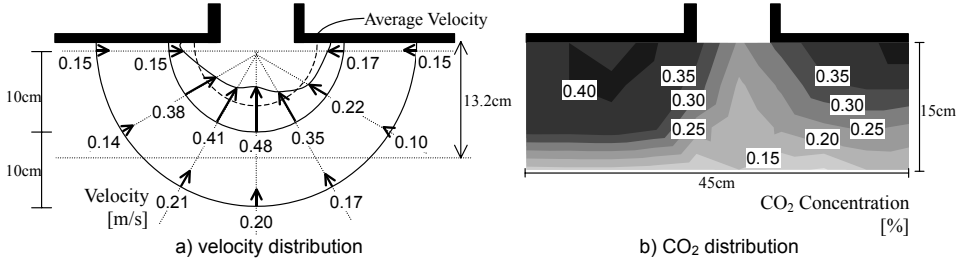

Figure 13 Velocity and CO_2 Distribution below Vent Opening (venting velocity = 2.45m/s, vent size 10cm x 10cm, point sink approximation)

CONCLUSION

Model scale experiments were carried to find the critical conditions for the onset of air entrainment and to predict the air entrainment ratio in quiescent two-layers environment. As a result, the followings are clarified.

1) Critical smoke layer thickness for the onset of air entrainment could be correlated by the power function of Froude number, which represents the venting velocity normalized by the hydrostatic head of smoke layer. The power is 2 for plane sink, 2/3 for line sink and 2/5 for point sink.

2) At the visible critical conditions, air entrainment ratio is approximately 0.2-0.4. To prevent air entrainment, smoke layer thickness must be more than 2.5 times of the critical smoke layer thickness determined by eye-observation.
3) Air entrainment ratio can be predicted by non-dimensional smoke layer thickness (actual smoke layer thickness / critical smoke layer thickness).

ACKNOWRIDGMENTS

This work has been financially supported by a grant-in-aid for scientific research offered by Ministry of Education, Culture, Sports, Science and Technology (Grant No. 12555163).

NOMENCLATURE

Alphabets

d	smoke layer thickness [m]	Fr	Froude number ($=v/(\Delta\rho g W/\rho_a)^{1/2}$)
g	gravity acceleration [m/s^2]	H	long edge length of vent opening [m]
R	radius of control volume [m]	T	temperature [^{o}C]
v	average venting velocity [m/s]	v'	induced air velocity [m/s]
W	short edge length of vent opening [m]	Y	carbon dioxide concentration [%]

Greek letters

ϕ	air entrainment ratio [-]	ρ	fluid density [kg/m^3]

Subscripts

a	lower air layer	*branch*	branch from line sink to point sink
cr	critical condition	*duct*	exhaust duct
s	upper smoke layer		

REFERENCES

[1] National Fire Protection Association, Venting Practices, Fire Protection Handbook 18th edition, pp.7-105–118, 1997
[2] Building Center of Japan, Shin Haien Setsubi Gijutu Shishin (Design Guidelines on Smoke Venting Equipment, New Edition, in Japanese), 1987
[3] Tanaka, T., Nakamura, K., A Model for Predicting Smoke Transport in Buildings, Report of the Building Research Institute, No. 123, 1989 (in Japanese)
[4] Peacock, R., D., Jones W., W., Forney, G., P., Portier, R., W., Reneke, P., A., Bokowski, R., W., Klote J., H., An Update Guide fro HAZARD I version 1.2, NISTIR 5410, National Institute of Standards and Technology, 1994
[5] Spratt D. and Heselden A. J. M.: "Efficient Extraction of Smoke from a Thin Layer under a Ceiling", Fire Research Note, No. 1001, 1974
[6] Davidian J. and Glover J. E.: "Development of the Non-Circulatory Waterspout", Journal of Hydraulic Division, Proc. ASCE, Vol.82, HY 4, 1038.3~1038.7, 1956